



This is a repository copy of *Crystal and electronic structures of A₂NaI₆ periodate double perovskites (A = Sr, Ca, Ba): candidate wasteforms for I-129 immobilization.*

White Rose Research Online URL for this paper:

<https://eprints.whiterose.ac.uk/169387/>

Version: Supplemental Material

Article:

O'Sullivan, S.E., Montoya, E., Sun, S.-K. et al. (7 more authors) (2020) Crystal and electronic structures of A₂NaI₆ periodate double perovskites (A = Sr, Ca, Ba): candidate wasteforms for I-129 immobilization. *Inorganic Chemistry*, 59 (24). pp. 18407-18419. ISSN 0020-1669

<https://doi.org/10.1021/acs.inorgchem.0c03044>

This document is the Accepted Manuscript version of a Published Work that appeared in final form in Inorganic Chemistry, copyright © American Chemical Society after peer review and technical editing by the publisher. To access the final edited and published work see <https://doi.org/10.1021/acs.inorgchem.0c03044>

Reuse

Items deposited in White Rose Research Online are protected by copyright, with all rights reserved unless indicated otherwise. They may be downloaded and/or printed for private study, or other acts as permitted by national copyright laws. The publisher or other rights holders may allow further reproduction and re-use of the full text version. This is indicated by the licence information on the White Rose Research Online record for the item.

Takedown

If you consider content in White Rose Research Online to be in breach of UK law, please notify us by emailing eprints@whiterose.ac.uk including the URL of the record and the reason for the withdrawal request.

Supporting Information

The crystal and electronic structures of A₂NaIO₆ periodate double perovskites (A=Sr,Ca,Ba): Candidate wasteforms for I-129 immobilisation

Sarah E. O'Sullivan^a, Eduardo Montoya^b, Shi-Kuan Sun^{a*}, Jonathan George^b, Cameron Kirk^c, Malin C. Dixon Wilkins^a, Philippe F. Weck^d, Eunja Kim^{e*}, Kevin S. Knight^a, and Neil C. Hyatt^{a*}.

^aDepartment of Materials Science and Engineering, University of Sheffield, Sheffield, S1 3JD, UK

^bDepartment of Chemistry and Biochemistry, University of Nevada, Las Vegas, NV 89154, USA

^cDepartment of Electrical and Computer Engineering, University of Nevada, Las Vegas, NV 89154, USA

^dSandia National Laboratories, Albuquerque, NM 87185, USA

^eDepartment of Physics and Astronomy, University of Nevada, Las Vegas, NV 89154, USA

*Corresponding authors. E-mail address: shikuan.sun@sheffield.ac.uk;
kimej@physics.unlv.edu; n.c.hyatt@sheffield.ac.uk. Here, Shi-Kuan Sun (shikuan.sun@sheffield.ac.uk) will handle correspondence at all stages

Table S1: Comparison of BVS as calculated in this work against calculations using bond length data from previous work [22].

Compound	Bonds	Expected valence	BVS from previous work	BVS from this work
Ba_2NaIO_6	Ba-O (CN=12)	2	1.980	1.967
	I-O (CN=6)	7	5.840	7.079
	Na-O (CN=6)	1	1.289	1.073
Sr_2NaIO_6	Sr-O (CN=12)	2	1.827	1.892
	I-O (CN=6)	7	5.854	7.077
	Na-O (CN=6)	1	1.341	1.125
Ca_2NaIO_6	Ca-O (CN=12)	2	2.008	1.876
	I-O (CN=6)	7	5.996	7.122
	Na-O (CN=6)	1	1.142	0.982

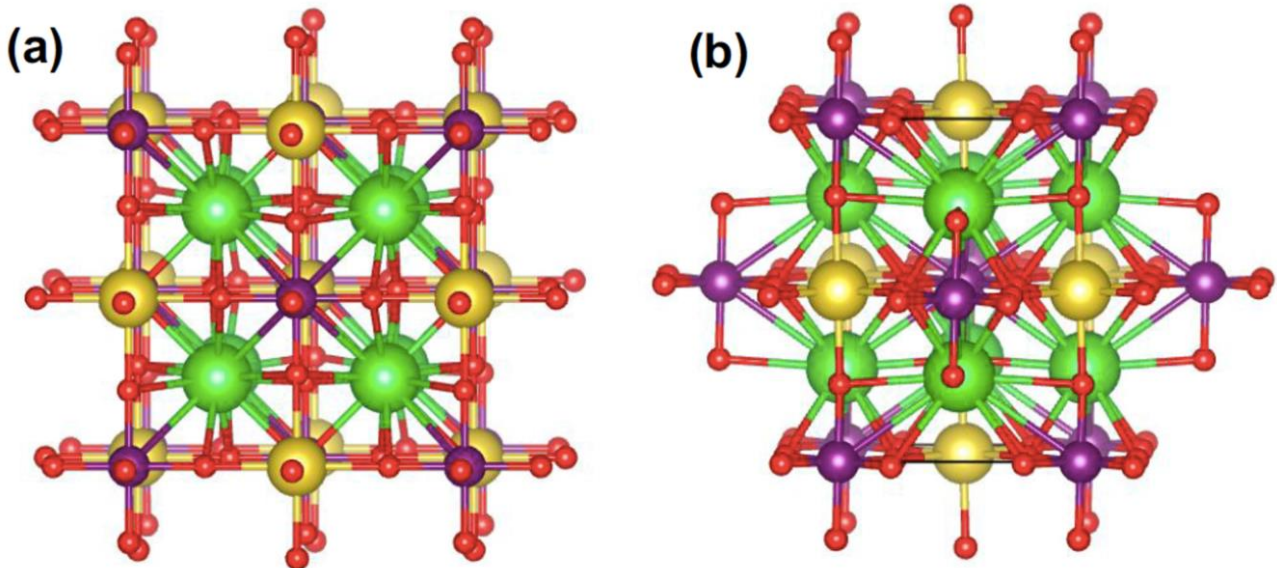


Figure S1: Ball-and-stick representation of the DFT-optimized (a) cubic *Fm*-3*m* phase (b) monoclinic *P*2₁/*n* phase. Colour legend: green, M = Ca, Sr, or Ba; yellow, Na; purple, I; red, O.

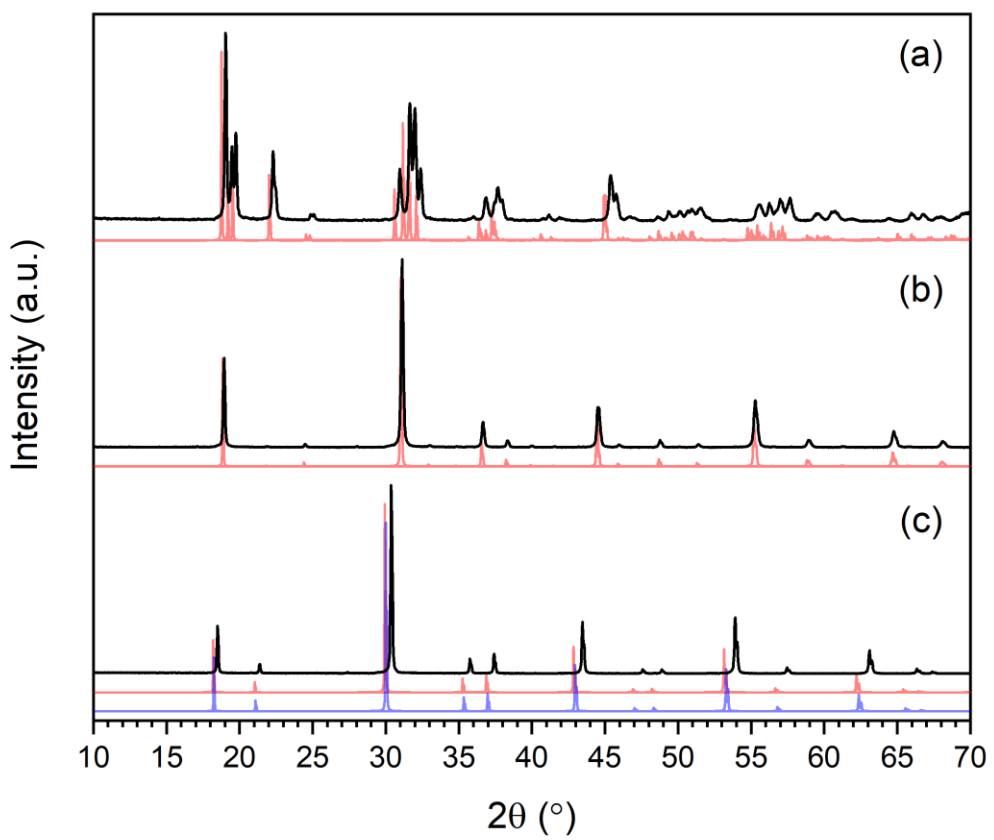


Figure S2: Simulated X-ray diffraction patterns of (a) Ca_2NaIO_6 in the monoclinic $P2_1/n$ phase, (b) Sr_2NaIO_6 in the monoclinic $P2_1/n$ phase, and (c) Ba_2NaIO_6 in the cubic $Fm-3m$ (red) and monoclinic $P2_1/n$ (blue) phases. Corresponding experimental XRD patterns collected in this study are displayed in black.

Table S2: Comparison of bond lengths obtained via DFT to experimental data acquired in this study (where applicable).

Ba₂NaIO₆ Fm-3m			Ba₂NaIO₆ P2₁/n			Sr₂NaIO₆ P2₁/n			Ca₂NaIO₆ P2₁/n		
Bond	DFT (Å)	Exp (Å)	Bond	DFT (Å)	Exp (Å)	Bond	DFT (Å)	Exp (Å)	Bond	DFT (Å)	Exp (Å)
Ba-O1 (x12)	2.992	2.954	Ba-O1	3.022	-	Sr-O1	3.186	3.186	Ca-O1	3.673	3.617
			Ba-O1	3.021	-	Sr-O1	2.658	2.658	Ca-O1	2.384	2.375
			Ba-O1	2.962	-	Sr-O1	2.553	2.550	Ca-O1	2.352	2.340
			Ba-O1	2.970	-	Sr-O1	3.248	3.248	Ca-O1	3.395	3.364
			Ba-O2	2.945	-	Sr-O2	2.571	2.571	Ca-O2	2.387	2.381
			Ba-O2	3.042	-	Sr-O2	2.790	2.790	Ca-O2	2.697	2.683
			Ba-O2	2.985	-	Sr-O2	2.875	2.875	Ca-O2	2.745	2.725
			Ba-O2	3.001	-	Sr-O2	3.366	3.366	Ca-O2	3.705	3.654
			Ba-O3	3.012	-	Sr-O3	2.820	2.819	Ca-O3	2.562	2.574
			Ba-O3	3.019	-	Sr-O3	2.556	2.556	Ca-O3	2.384	2.366
			Ba-O3	2.976	-	Sr-O3	3.398	3.398	Ca-O3	3.703	3.671
			Ba-O3	2.968	-	Sr-O3	2.846	2.846	Ca-O3	3.020	2.961
I-O1 (x6)	1.908	1.868	I-O1 (x2)	1.909	-	I-O1 (x2)	1.863	1.863	I-O1 (x2)	1.905	1.861
			I-O2 (x2)	1.909	-	I-O2 (x2)	1.869	1.870	I-O2 (x2)	1.900	1.865
			I-O3 (x2)	1.908	-	I-O3 (x2)	1.874	1.874	I-O3 (x2)	1.910	1.874
Na-O1 (x6)	2.314	2.298	Na-O1 (x2)	2.315	-	Na-O1 (x2)	2.281	2.281	Na-O1 (x2)	2.353	2.341
			Na-O2 (x2)	2.318	-	Na-O2 (x2)	2.275	2.275	Na-O2 (x2)	2.287	2.297
			Na-O3 (x2)	2.315	-	Na-O3 (x2)	2.286	2.286	Na-O3 (x2)	2.369	2.368

Table S3: Atomic positions obtained via DFT and compared to experimental values for Ca_2NaIO_6 ($P2_1/n$), Sr_2NaIO_6 ($P2_1/n$), and Ba_2NaIO_6 ($Fm-3m$ and $P2_1/n$).

$\text{Ca}_2\text{NaIO}_6 P2_1/n$							
Atom	Wyckoff position	x		y		z	
		DFT	Exp	DFT	Exp	DFT	Exp
Na	2a	0	0	0	0	0	0
I	2b	0	0	0	0	0.5	0.5
Ca	4e	0.018	0.0160	0.558	0.5575	0.243	0.2447
O1	4e	-0.114	-0.1108	-0.057	-0.0537	0.278	0.2809
O2	4e	0.222	0.2243	0.324	0.3266	0.046	0.0453
O3	4e	0.335	0.3381	0.768	0.7666	0.072	0.0705
$\text{Sr}_2\text{NaIO}_6 P2_1/n$							
Atom	Wyckoff position	x		y		z	
		DFT	Exp	DFT	Exp	DFT	Exp
Na	2a	0	0	0	0	0	0
I	2b	0	0	0	0	0.5	0.5
Sr	4e	0.010	0.0057	0.544	0.5287	0.249	0.2499
O1	4e	-0.080	-0.0665	-0.028	-0.0177	0.278	0.2762
O2	4e	0.238	0.2433	0.315	0.3071	0.038	0.0331
O3	4e	0.320	0.3124	0.761	0.7608	0.047	0.0355
$\text{Ba}_2\text{NaIO}_6 Fm-3m$							
Atom	Wyckoff position	x		y		z	
		DFT	Exp	DFT	Exp	DFT	Exp
I	4a	0	0	0	0	0	0
Na	4b	0.5	0.5	0.5	0.5	0.5	0.5
Ba	8c	0.25	0.25	0.25	0.25	0.25	0.25
O1	24e	0.226	0.224	0	0	0	0
$\text{Ba}_2\text{NaIO}_6 P2_1/n$							
Atom	Wyckoff position	x		y		z	
		DFT	Exp	DFT	Exp	DFT	Exp
Na	2d	0.5	-	0.0	-	0.0	-
I	2a	0.0	-	0.0	-	0.0	-
Ba	4e	-0.25	-	0.5	-	0.0	-
O1	4e	-0.005	-	0.775	-	0.226	-
O2	4e	0.226	-	-0.001	-	0.008	-
O3	4e	-0.004	-	0.227	-	0.225	-

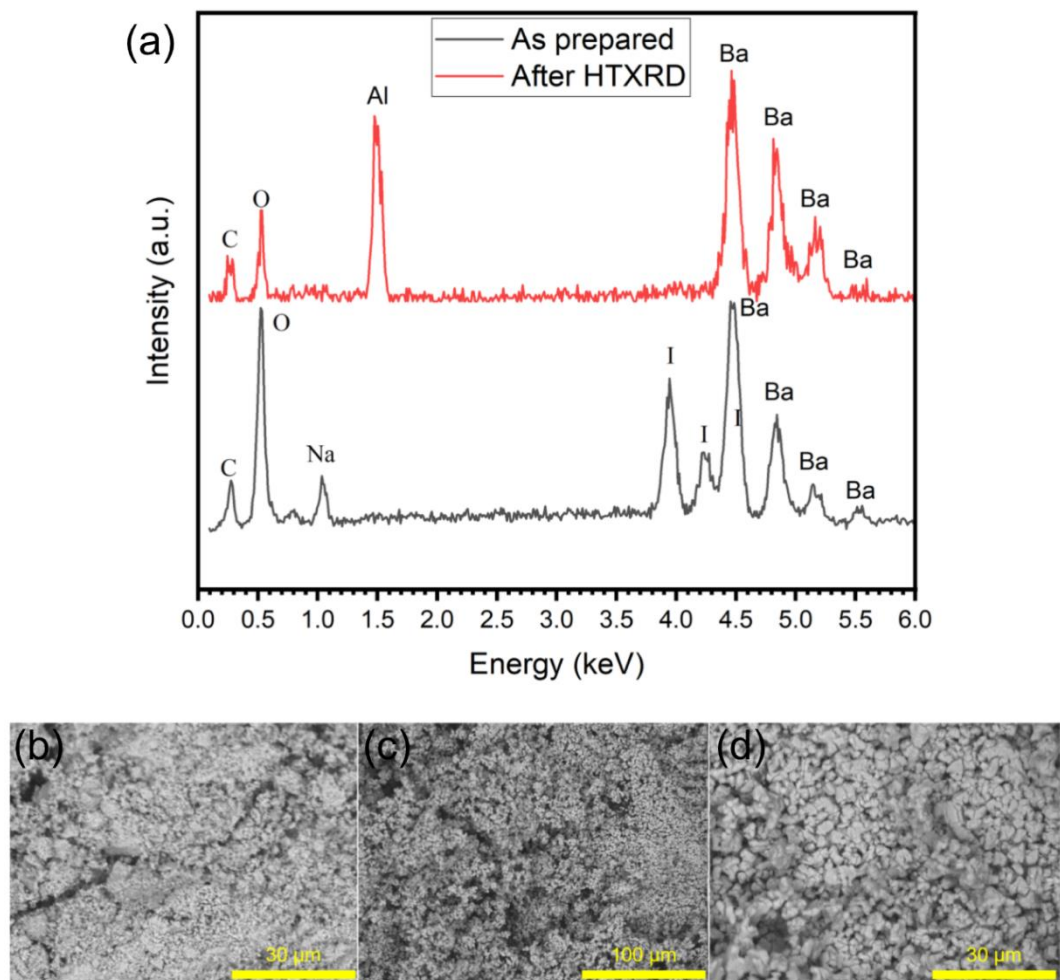


Figure S3: a) EDS analysis of Ba_2NaIO_6 powder pre- (black) and post- HT-XRD (red) showing the loss of Na and I after the heat treatment. The inclusion of Al is attributed to contamination arising from the Al_2O_3 crucible reacting under a combined heat treatment with a mild iodine flux. SEM images show as prepared Ba_2NaIO_6 ((b)) and after decomposition at $1030\text{ }^\circ\text{C}$ to BaO ((c) and (d)).

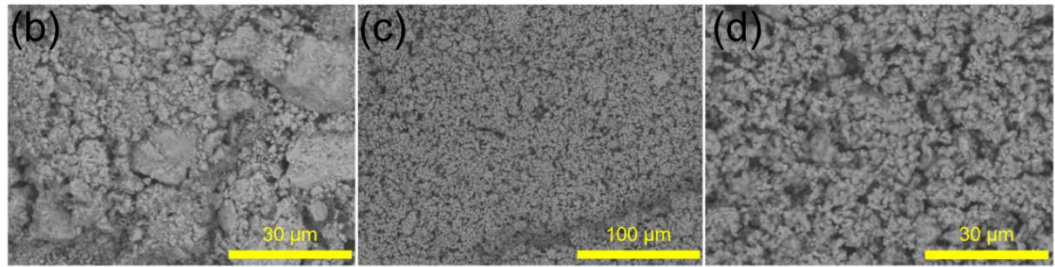
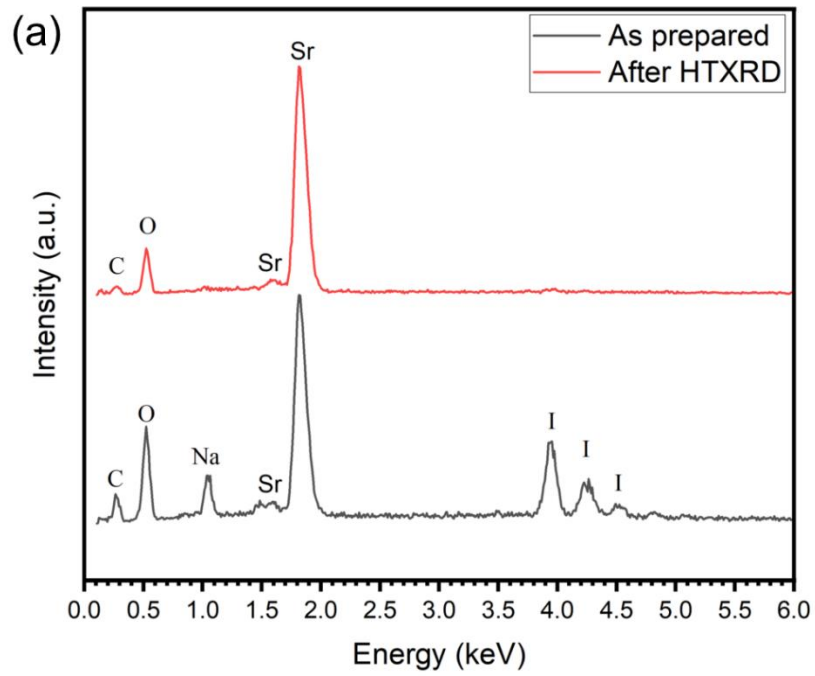


Figure S4 a) EDS analysis of Sr_2NaIO_6 powder pre- (black) and post- HT-XRD (red). SEM images show prepared Sr_2NaIO_6 (b) and after decomposition at $950\text{ }^\circ\text{C}$ to SrO ((c) and (d)).

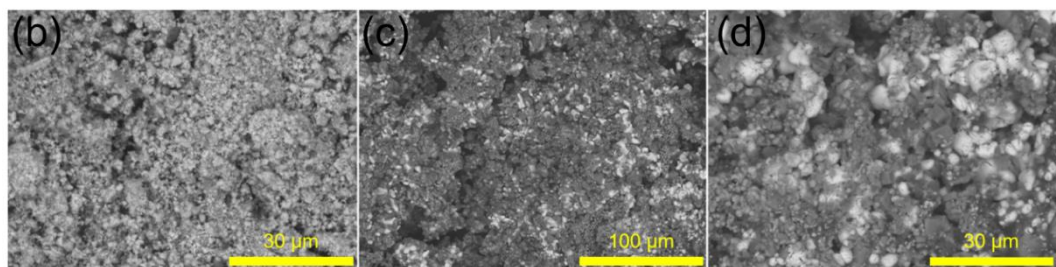
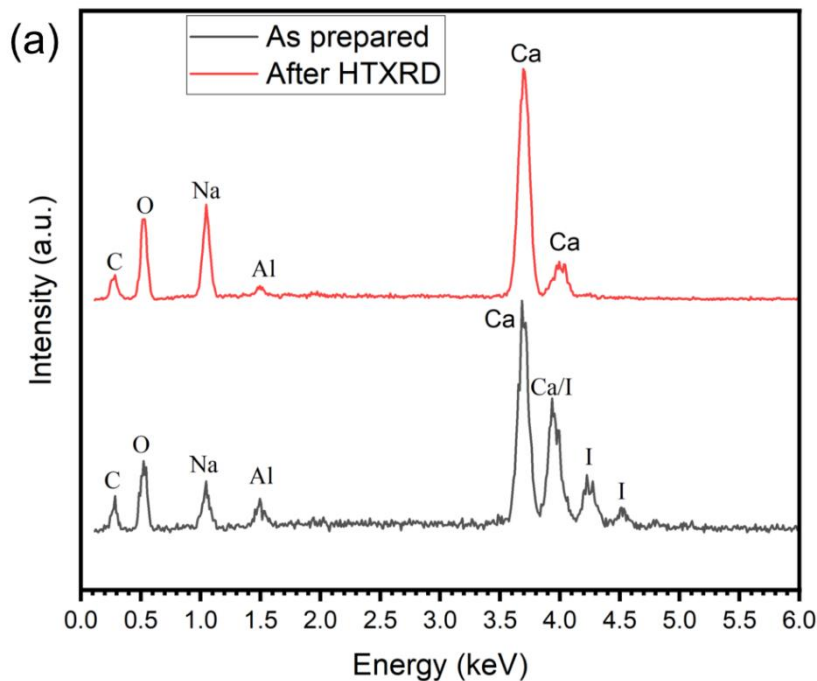


Figure S5: a) EDS analysis of Ca_2NaIO_6 powder pre- (black) and post- HT-XRD (red). A small amount of Sr contamination is visible both before and after HT-XRD. SEM images show as prepared Ca_2NaIO_6 (b) and after decomposition at 750°C to CaO ((c) and (d)).